Acta Cryst. (1990). B46, 599–609

Structural Analysis of Hollandite $Ba_xTi^{3+}_{2x}Ti^{4+}_{8-2x}O_{16}$ with $x = 1{\cdot}07$ and $1{\cdot}31$ from 5 to 500 K*

BY ROBERT W. CHEARY

School of Physical Sciences, University of Technology Sydney, PO Box 123, Broadway, New South Wales, Australia 2007

(*Received* 2 *August* 1989; *accepted* 1 *June* 1990)

Abstract

Neutron powder diffraction data for barium hollandites $Ba_xTi_8O_{16}$ ($x = 1{\cdot}07$ and $1{\cdot}31$) have been refined at temperatures from 5 to 400 K for $x = 1{\cdot}07$ and from 160 to 500 K for $x = 1{\cdot}31$. These compounds undergo monoclinic $I2/m$ to tetragonal $I4/m$ phase transformations at 375 (5) K ($x = 1{\cdot}07$) and 475 (10) K ($x = 1{\cdot}31$) which display first-order characteristics. The cell volumes are discontinuous along with the thermal-expansion coefficients at the transition temperatures. Below each transition temperature the metastable tetragonal phase and the monoclinic phase coexist with the proportion of monoclinic increasing slightly at low temperatures. This transformation resembles the martensitic monoclinic–tetragonal transformation in ZrO_2. Multiphase Rietveld refinement was carried out to determine the structural parameters of both phases. On transition to tetragonal the major contribution to the contraction of the cell volume is the contraction of the tunnel cavities; the O octahedra forming the tunnel walls undergo expansion. This process derives from a relaxation of the shear strain on the tunnel walls. Various temperature-dependent properties of the structures are discussed, particularly the tunnel distortion and the ⟨Ti—O⟩ bond lengths. The capacity of the tunnel cavities in these and related hollandites to accommodate Cs from nuclear waste is also discussed.

Introduction

SYNROC is one of a number of synthetic minerals being developed as a solid matrix for nuclear waste encapsulation. In this material there are essentially four parent phases; these are hollandite, perovskite, hibonite and zirconolite (Fielding & White, 1987). Hollandite, the subject of the present paper, constitutes approximately 30% of SYNROC and is included principally to immobilize radionuclides of Cs and, to a lesser extent, Ba and Rb. The general unit-cell formula of the host barium hollandite in SYNROC is $Ba_x[(Ti^{3+}_{\alpha}Al^{3+}_{1-\alpha})_{2x}Ti^{4+}_{8-2x}]O_{16}$, where x, the Ba concentration in the hollandite tunnels, can range from 1·08 up to 1·33 depending on the Ti^{3+}/Al^{3+} ratio (Kesson & White, 1986). In barium aluminous hollandites (*i.e.* $\alpha = 0$) the Ba concentration can be varied from 1·14 to 1·23 ions per cell (Roth, 1981; Cheary, 1986). When Ti^{3+} ions are introduced into the walls of the hollandite tunnels alongside Ti^{4+} and Al^{3+} ions, the lower limit for x drops to approximately 1·08, but in the absence of Al^{3+} it reverts to 1·14 Ba per cell (*i.e.* $Ba_{1{\cdot}14}Ti_8O_{16}$). In the synthetic hollandites $Ba_x(Ti^{4+}/M^{3+})_8O_{16}$ with M = Al, Sc, Cr, Ga, Ru and In, x is never less than 1·12 and never exceeds 1·33 (Zanderbergen, Everstijn, Mijlhoff, Renes & Ijdo, 1987). In other Ba hollandites of this type the upper limit is also 1·33 (Bursill & Grzinic, 1980; Cheary & Squadrito, 1989) and it is expected that this will be the case for $Ba_xTi_8O_{16}$ hollandite. Higher occupancy levels up to $x = 1{\cdot}46$, are achieved in barium hollandites when the Ti^{4+} ion is replaced by a larger ion such as Sn^{4+} (Cadee & Verschoor, 1978; Zanderbergen *et al.*, 1987).

The Ba concentration in a hollandite can be estimated from the position of the superlattice lines in the X-ray or electron diffraction patterns. These lines form because of the ordering of the Ba along the tunnels. For Ba hollandites the superlattice multiplicity m increases from 4·6–4·7 up to 5·7–6·0 over the complete solid-solution range, $x = 1{\cdot}14$ to 1·33 (Kesson & White, 1986). In $Ba_x(Mg_xTi_{8-x})O_{16}$, this is manifested as a large shift in the first major X-ray superlattice line from $2\theta \simeq 29°$ at $x = 1{\cdot}14$ to $2\theta \simeq 32°$ at $x = 1{\cdot}33$ using Cr $K\alpha$ radiation (Cheary & Squadrito, 1989). When perfect long-range order exists in the structure the multiplicity m is related to the Ba concentration by the equation $m = 7{\cdot}5x - 4$ (Mijlhoff, Ijdo & Zanderbergen, 1985), and this relation may be used in reverse to identify the Ba concentration. Although small deviations can occur at either end of the solid-solution range through the formation of microdomains (Cheary & Squadrito, 1989), the accuracy with which x can be determined

* The neutron powder data for this work were collected at the Institut Laue–Langevin, Grenoble, France.

0108-7681/90/050599-11$03.00

from the multiplicity m or the 2θ position of the superlattice lines is approximately $\pm 0{\cdot}04$.

In general, aluminium-rich SYNROC hollandites such as $Ba_{1{\cdot}14}Al_{2{\cdot}28}Ti_{5{\cdot}72}O_{16}$ are tetragonal (space group $I4/m$) and the unit cells are smaller than Ti^{3+}-rich hollandites. As Al^{3+} is replaced by Ti^{3+} the unit cell distorts to monoclinic and the space group becomes $I2$ or $I2/m$. Schmactel & Muller-Buschbaum (1980) have carried out a structural refinement based on single-crystal X-ray data from a hollandite with the supposed composition $BaTi_8O_{16}$. They assumed the space group to be $I2$ and reported lattice parameters indicating a significant monoclinic distortion with $a = 10{\cdot}309$, $b = 2{\cdot}971$, $c = 9{\cdot}981$ Å and $\beta = 91{\cdot}1°$. Although the lattice parameters quoted by Kesson & White (1986) for $Ba_{1{\cdot}14}Ti_8O_{16}$ are also monoclinic ($a = 10{\cdot}201$, $b = 2{\cdot}958$, $c = 10{\cdot}179$ Å and $\beta = 90{\cdot}7°$), the distortion, reflected by β and the difference in the lattice parameters a–c, is not as large as for $BaTi_8O_{16}$. On the basis of normal Ba hollandite behaviour (Cheary, 1986; Zanderbergen *et al.*, 1987; Cheary & Squadrito, 1989), the distortion should be greater in $Ba_{1{\cdot}14}Ti_8O_{16}$ owing to the higher concentration of Ti^{3+} in the tunnel walls. The source of this inconsistency is that Schmactel & Muller-Buschbaum (1980) assumed a composition of 1 Ba per unit cell which was not verified either chemically or by X-ray refinement. In fact, since that time no Ba hollandite has been synthesized with 1 Ba per unit cell. The lattice parameters of their '$BaTi_8O_{16}$' single crystal are consistent with an actual composition between 1·20 and 1·33 Ba per cell. Given this error there is a distinct possibility that the structural parameters of Schmactel & Muller-Buschbaum (1980) are also slightly in error.

The purpose of the present study is to determine the structural characteristics of the Ba hollandite $Ba_x(Ti^{3+}_{2x}Ti^{4+}_{8-2x})O_{16}$ at different Ba concentrations and over a range of temperatures from 5 to 500 K. This group of hollandites is of particular interest to the SYNROC program because of the strong correlation between the presence of Ti^{3+} ions and the extent to which Cs can be substituted for Ba. In $Ba_x(Al_{2x}Ti_{8-x})O_{16}$ hollandite with only Ti^{4+} ions in the structure, the level of Cs substitution for Ba is limited to 0·25 Cs per unit cell (Cheary, 1987), but when Ti^{3+} ions are present and the preparation is carried out under reducing conditions, up to 1·50 Cs can be incorporated within the unit cell. It is therefore of central importance to establish how the presence of Ti^{3+} in the oxygen octahedra affects the environment of the Ba ions within the tunnels of the structure. Of equal importance is an understanding of the factors which control hollandite stability. It is known that many monoclinic hollandites undergo the transition to tetragonal with increasing temperature [*e.g.* $Ba_{1{\cdot}14}(Mg_xTi_{8-x})O_{16}$, Roth (1981)], but the manner in which the structural parameters change has not been previously examined. Cheary & Squadrito (1989) have suggested that Mg and Ti are not randomly distributed amongst the octahedral sites and that the monoclinic distortion is closely linked with the tunnel walls containing differing proportions of Ti and Mg. Assuming this to be the case, the transformation from the high-temperature tetragonal phase to the monoclinic phase would be a diffusion-controlled process. This is by no means certain and further studies are clearly needed to identify the mechanics of the transformation. In the present work two hollandite specimens were prepared one at each end of the composition range with nominal compositions '$Ba_{1{\cdot}14}Ti_8O_{16}$' and '$Ba_{1{\cdot}33}Ti_8O_{16}$'. Rietveld refinement of the neutron powder patterns from these specimens was carried out for a range of specimen temperatures encompassing each of the monoclinic–tetragonal transitions.

General features of the hollandite structure

All the hollandites discussed in this work are represented by the non-standard space group $I2/m$. This is done to simplify the comparison of results from monoclinic hollandites and tetragonal hollandites (which are normally represented by the space group $I4/m$). The unique axis or tunnel axis is along the **b** direction. A projection of the hollandite structure looking down the **b** axis showing the pattern of

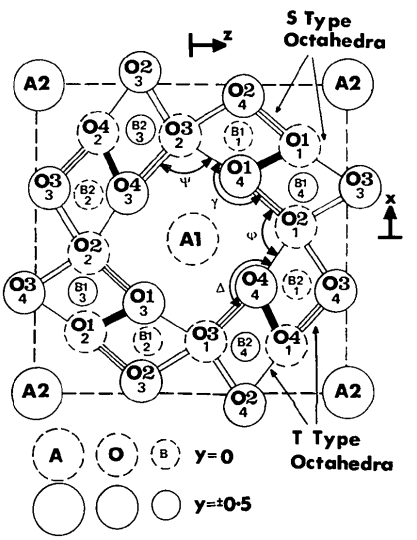

Fig. 1. Projection of the hollandite structure looking down the b-axis tunnels showing the various atomic positions and tunnel angles referred to in the paper. The two different types of octahedra are labelled S and T. The O—O bonds depicted with similar line patterns possess the same bond length in tetragonal hollandites, but in monoclinic hollandites this is only true for opposing sides of the tunnel.

one-dimensional tunnels and tunnel walls is illustrated in Fig. 1. Expressed in terms of available sites the unit-cell composition is $A_2B_8O_{16}$ where B represents sites within oxygen octahedra filled, in the case of SYNROC hollandites, by a combination of Ti^{4+}, Ti^{3+} and Al^{3+} ions. The A sites are in the tunnels and only partially occupied by Ba ions, normally from 57% at $x = 1{\cdot}14$ up to 66·7% at $x = 1{\cdot}33$. Each Ba is located in a box-shaped cavity of eight O atoms which is normally larger than the cation. The Ba can occupy either a central position or one of two possible off-centre positions (*i.e.* 0, $\pm y$, 0 with $y \sim 0{\cdot}1$ to 0·2) depending on whether or not the A sites either side of the particular A site are filled. When one adjacent site is filled and the other is empty, the atom in the central site will experience an off-centre electrostatic force and be displaced. Each tunnel in a hollandite is identical and defined by four walls of oxygen octahedra, referred to here as octahedral walls, linked together by corner sharing (see Kesson, 1983). In tetragonal hollandites all the oxygen octahedra are identical, but in monoclinic hollandites only those on opposite walls are identical. The two different types in the monoclinic case are called S and T types as shown in Fig. 1. In the transformation from tetragonal to monoclinic the most noticeable change to the structure is in the hinge angles between the tunnel walls, ϕ and ψ (projected onto the 010 plane). In tetragonal hollandites these angles are the same and typically about 97° but, on transformation to monoclinic ϕ increases, sometimes by 7–8°, and ψ decreases by about the same amount. When a tetragonal→monoclinic transition is induced by increasing the average size of the B ions each tunnel wall rotates as a rigid framework about hinges at the corners between adjacent walls and parallel to the tunnel axis. The whole process is analogous to distorting a square into a rhombus. This is a somewhat simplified picture and in practice some deformation of the tunnel wall occurs which is evidenced by a change in the deformation angles Δ and δ (projected on the 010 plane).

Preparation and identification procedures

Two specimens were prepared for neutron diffraction corresponding to the end members of the barium titanium hollandite family, nominally $Ba_{1{\cdot}14}Ti_8O_{16}$ and $Ba_{1{\cdot}33}Ti_8O_{16}$. Before preparing these specimens a number of preliminary specimens were prepared to identify suitable firing conditions. In the final specimens pre-dried starting materials $BaCO_3$ and TiO_2 were carefully weighed out and then thoroughly mixed by wet grinding an agate ball mill. The slurry was then dried, compacted into discs and calcined at 1100 K for 4 h in air. The weight losses on calcination agreed to within 0·2% of the expected values. Both specimens were ground up and calculated quantities of fine graphite powder blended in to act as the reducing agent for the conversion of Ti^{4+} to Ti^{3+}. The final firing was carried out at 1540 K for 16 h in an atmosphere of 5% hydrogen in nitrogen with the specimens being allowed to cool naturally to room temperature over a period of 36 h within the furnace.

Rapid X-ray diffraction scans of the final products over the range $2\theta = 20$–45° with Cu $K\alpha$ radiation appeared to be single-phase monoclinic hollandites. Examination of the neutron diffraction data collected over a greater angular range at a later time, revealed this not to be the case and both samples were found to be two-phase mixtures consisting of a monoclinic hollandite and a metastable tetragonal hollandite. This was confirmed by carrying out X-ray diffraction scans over a similar 2θ range on both a laboratory powder diffractometer and on the high-resolution Debye–Scherrer diffractometer at the Daresbury Synchrotron Laboratory where the full width at half maximum intensity (FWHM) of the diffraction lines is approximately 0·04° 2θ up to $2\theta \simeq 100°$. (Note: FWHM is typically 0·1 to 0·15° 2θ on a laboratory diffractometer.) The fact that the samples were mixtures was not immediately recognized as the tetragonal lines are embedded within the monoclinic lines at low 2θ angles. In particular, $Ba_{1{\cdot}14}Ti_8O_{16}$ is very close to the monoclinic–tetragonal phase boundary (Kesson & White, 1986) and the 'monoclinic splitting' of the diffraction lines shows up as shoulders at low angles rather than distinct peaks. Well-resolved superlattice lines were present in the X-ray patterns of both specimens but at different 2θ angles. In addition, a number of weak unidentified impurity lines were observed at the 1–2% level. This is consistent with the Ba occupancies given by refinement of the neutron data which were slightly less than the values expected from the amounts of starting materials used. The actual compositions given by the neutron data were $Ba_{1{\cdot}07\pm0{\cdot}03}Ti_8O_{16}$ and $Ba_{1{\cdot}31\pm0{\cdot}03}Ti_8O_{16}$ rather than $Ba_{1{\cdot}143}Ti_8O_{16}$ and $Ba_{1{\cdot}33}Ti_8O_{16}$, respectively. Hereinafter the two specimens will be referred to as the Ba(1·07) and Ba(1·31) hollandites.

Neutron powder diffraction data were collected for both specimens over the angular range $2\theta =$ 0–160° using the high-resolution diffractometer D2B at the Institut Laue–Langevin. The design and resolution function of this 64 detector diffractometer are discussed in Hewat (1986). In the present experiment the instrument was operated at $\lambda = 1{\cdot}59327$ Å and over the measured 2θ range the FWHM of the diffraction lines decreases steadily from 0·45° 2θ at $2\theta = 12°$ to a minimum of 0·35° 2θ at $2\theta = 100°$ before rising once again to ~0·6° 2θ at $2\theta = 150°$. The wavelength quoted here was obtained by

refining neutron data from a fine Ni powder at 298 K with the lattice parameter assumed to be 3·52387 Å (Wyckoff, 1963). In preparation for measurement approximately 12 g of each hollandite was ground into a powder fine enough to pass through a 38 μm sieve before being packed and sealed in a thin-walled V can. For measurements between 5 and 300 K the can was loaded into a continuous-flow He cryostat. A cryofurnace was employed above this range and up to 500 K. Data were collected from the Ba(1·07) hollandite at 5, 100, 200, 300 and 400 K in that order. Fewer temperatures were examined for the Ba(1·31) hollandite, namely 160, 298, 400 and 500 K.

At the highest temperature only, each specimen is a single-phase tetragonal hollandite. The monoclinic–tetragonal transition occurs between 300 and 400 K in Ba(1·07) and between 400 and 500 K in Ba(1·31). The actual transition temperatures quoted later in this paper were determined first on the high-intensity, low-resolution energy-dispersive X-ray diffractometer (Clark, 1989) at the SERC Synchrotron, Daresbury, England. X-ray diffraction patterns were recorded at 10 K intervals from 300 to 450 K for Ba(1·07) and from 350 to 520 K for Ba(1·31). Despite the poor resolution of this diffractometer, which is unable to resolve the monoclinic splitting, it is possible to identify the transition temperatures by the change in the gradient dE/dT of the diffraction line energy E with temperature T. The transition temperatures obtained were 373 ± 5 K for the Ba(1·07) and 478 ± 10 K for the Ba(1·31) hollandite where the errors reflect the reproducibility of the method using different diffraction lines. To confirm these temperatures a second measurement was carried out on a standard horizontal X-ray powder diffractometer set up with Cu $K\beta$ radiation. X-ray count data for 600/006 monoclinic lines along with the 600 tetragonal line were collected by step scanning at intervals of 0·01° 2θ and at temperatures ranging from 100 K below the transition to 50 K above the transition at intervals of 10 K. At approximately 50 K below the transition the three lines are not clearly resolved. The transition temperature T_c was therefore identified by plotting the peak height of the triplet against temperature. As the lines merge the peak height rises uniformly but above T_c it remains substantially constant; T_c is therefore identified as the intersection of these two regions. The transition temperatures obtained by this method were 378 ± 8 K for Ba(1·07) and 475 ± 8 K for Ba(1·31). In view of the difference in the two sets of results for T_c, the transition temperatures assumed are 375 ± 5 K for Ba(1·07) and 475 ± 10 K for Ba(1·31).

As indicated earlier, close inspection of the neutron data from D2B below the transition temperatures revealed that neither specimen was a single-phase hollandite. Two coexisting hollandite phases were identified in each case; one monoclinic and the other tetragonal. This is most clearly illustrated in an X-ray scan (Fig. 2) obtained using the high-resolution synchrotron diffractometer 9·3 at the Daresbury Laboratory, which shows well-resolved 600/006 monoclinic lines either side of the 600 tetragonal line. On cooling through the transformation not all the tetragonal phase converts to monoclinic. The rate of transformation from tetragonal to monoclinic is slow and the proportion of monoclinic phase does not noticeably increase with time at any fixed temperature, but does increase with decreasing temperature. This was inferred from the neutron intensities of the monoclinic lines relative to related tetragonal lines which are greater at 5 K than at 300 K and do not change with time. Throughout this work the compositions of the tetragonal and monoclinic phases within each specimen are assumed to be the same. A number of factors support this claim. X-ray microprobe analysis on a JOEL 35C scanning electron microscope revealed no significant variation in the ratio of the intensities of the Ba L and Ti K line emissions at a large number of probe points in each sample. Also, chemical homogeneity was evident from the sharpness and 2θ positions of the X-ray superlattice lines. With Cu $K\beta$ radiation (λ = 1·3922 Å), the strong superlattice line at $2\theta = 17{\cdot}50°$ in Ba(1·07) and at $2\theta = 18{\cdot}50°$ in Ba(1·31) has a FWHM $\simeq 0{\cdot}18°$ 2θ which can be accounted for by instrumental effects, the presence of microdomains in the structure (Cheary & Squadrito, 1989) and the fact that this line is a $0k1/1k0$ doublet in the monoclinic phase. A difference in the composition between the tetragonal and monoclinic phases in room temperature Ba(1·31) of 0·05 Ba per cell say, would produce a pair of superlattice lines separated by

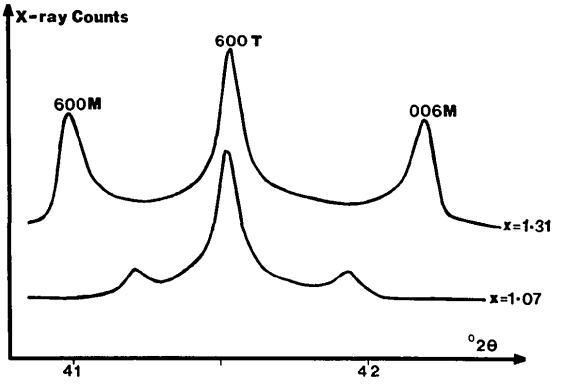

Fig. 2. X-ray powder diffraction scan at 1·1279 Å from $Ba_xTi_8O_{16}$ at x = 1·07 and 1·31 showing the 600 lines from the tetragonal phase and the 600 and 006 lines from the co-existing monoclinic phase. This data was collected from the high-resolution Debye–Scherrer diffractometer at the Daresbury Synchrotron Laboratory, England.

approximately 0·2° 2θ which would easily be resolved by the X-ray diffractometers used in this work. Further support for homogeneity is given by the fact that each tetragonal line is always located more or less centrally within the group of two or four monoclinic lines of related *hkl* (*e.g.* as in Fig. 2). Also, below each transition temperature the 020 lines of the tetragonal and monoclinic phases can just be resolved but above T_c these lines are coincident indicating that the b parameters are the same when the specimens are totally tetragonal. Close examination of both X-ray and neutron patterns at high 2θ angles for $T > T_c$ revealed no evidence of a two-phase material and the resolution in each type of pattern was comparable to any well-crystallized standard material. All these factors support uniformity of composition in these mixed-phase samples.

Rietveld refinement of the neutron powder data was carried out using the program developed by Wiles & Young (1981) and extensively modified by Howard & Hill (1986). In the present analysis the diffraction profiles were fitted by a pseudo-Voigt function in which the pseudo-Voigt parameter γ was fitted to a polynomial $\gamma = \gamma_0 + \gamma_1 2\theta + \gamma_2 2\theta^2$. A zero 2θ error was included in the refinement along with an asymmetry term developed to model axial divergence (Howard, 1982) and the background BKG was fitted to a polynomial of the form $\mathrm{BKG} = b_0 + b_1 2\theta + b_2 2\theta^2 + b_3/2\theta$. Although both specimens contained weak impurity lines, these were excluded from the refinement even though there was no overlap with hollandite lines. With the exception of excluded regions each pattern was refined over the 2θ range 10–150°. To facilitate comparison between the tetragonal and monoclinic structural data, all the hollandite phases were refined under the coordinate scheme for *I*2/*m* defined in Cadee & Verschoor (1978). Constraints were imposed on the lattice parameters and atomic coordinates of the tetragonal components to reflect *I*4/*m* symmetry and the b axis was taken as the unique axis. The goodness of fit indicators quoted with the refined data in Table 1 are the weighted pattern R factor R_{wp}, its expected value R^E_{wp} (based on counting statistics) and the Bragg factor R_B as defined in Howard & Hill (1986). The expected standard deviations (e.s.d.'s) of the refined structural parameters, lattice parameters and instrumental terms calculated by the Rietveld program and quoted in Table 1 represent the precision of the parameters a_i calculated from the effects of Poisson intensity statistics,

$$\sigma^2(a_i) = \sum_{j=1}^{N} (\partial a_i/\partial y_j)^2 \sigma^2(y_j)$$

where y_j is the observed neutron count at $2\theta_j$. In the case of the lattice parameters the e.s.d.'s should be reasonable estimates of their accuracy as well as their precision, as the major systematic errors of the diffractometer affecting the line position are modelled in the refinement and the diffractometer wavelength was calibrated with Ni powder.

Refinement of the Ba(1·07) and Ba(1·31) neutron data at 400 and 500 K respectively, was relatively straightforward as the specimens were single-phase tetragonal. Isotropic temperature factors were assigned to the Ti and O atoms. Anisotropic temperature parameters were adopted for Ba but constrained to the *I*4/*m* conditions, $\beta_{11} = \beta_{33}$ and $\beta_{12} = 0$. This was necessary to accommodate any positional disorder of the Ba atoms in the tunnel direction. In addition the Ba atoms were assumed to be randomly distributed over the off-centre A sites. Owing to the strong correlation between β_{22} and the off-centre shift y, very little significance can be attached to the absolute values of these terms. R_{wp} or R_B could be kept constant by maintaining $u_{22} + y \simeq$ constant where u_{22} is the effective r.m.s. displacement along the tunnel direction expressed as a fraction of b and given by $(\beta_{22}/2\pi^2)^{1/2}$. When β_{22}, y and the Ba occupancy were refined simultaneously, instability was introduced into the refinement. By alternately fixing y or β_{22} convergence occured readily and a reproducible value for the Ba occupany in each specimen could be obtained independently of the starting value for y or β_{22}. It is worth remarking that no improvement of the fit was obtained when Ba was split between off-centre sites and a central A site. Although this has been achieved with X-ray single-crystal data (*e.g.* Fanchon, Vicat, Hodeau, Wolfers, Tran Qui & Strobel, 1987) it is not effective here because the contribution of Ba to the total scattering is significantly smaller for neutrons.

For specimens containing a mixture of tetragonal and monoclinic phases, a two-phase refinement was carried out with independent coordinates and isotropic thermal parameters assigned to the Ti and O ions in each phase. It was not possible to obtain physically realistic values with independent parameters assigned to Ba in each phase. As indicated earlier, the approach adopted was to assume that the Ba occupancy in the tetragonal and monoclinic phases is the same and unchanged from that of the high-temperature specimens. Also, the off-centre shift y and thermal parameters of Ba were also assumed to be the same and constrained to the *I*4/*m* condition even in the monoclinic phase.

With the scheme described above, acceptable fits were obtained for all the specimens with R_B from 1·7 to 3·9% and R_{wp} from 7 to 10% for expected values R^E_{wp} between 2 and 3%. The level of fitting achieved from the present data is typical of the instrument, which gives profile shapes that cannot be accurately modelled at low 2θ angles. Even with a fine Ni

Table 1. *Structural parameters for the barium hollandites* $Ba_xTi_8O_{16}$ (x = 1·07 *and* 1·31) *obtained by Rietveld refinement of high-resolution neutron powder data* (λ = 1·59327 Å) *collected over a range of temperatures from* 5 *to* 500 K

		$Ba_{1\cdot07\pm0\cdot03}Ti_8O_{16}$					$Ba_{1\cdot31\pm0\cdot03}Ti_8O_{16}$			
		5 K	100 K	200 K	300 K	400 K	160 K	298 K	400 K	500 K
Fit	R_{wp} (%)	9·8	9·5	8·5	6	6·8	9·3	8·0	5·8	7·2
	R_{wp}^E (%)	1·9	1·9	2·1	2·3	2·5	2·3	2·5	2·2	2·6
Ba	y	0·082 (10)	0·072 (12)	0·020 (10)	0·062 (5)	0·094 (4)	0·099 (11)	0·131 (6)	0·114 (7)	0·167
	u_{22}/b	0·113 (16)	0·124 (10)	0·087 (10)	0·076 (6)	0·099 (10)	0·149 (16)	0·120 (17)	0·125 (10)	0·111 (10)
	B (Å^2)	4·6 (1·0)	4·8 (7)	3·9 (4)	3·6 (3)	4·7 (6)	4·7 (8)	4·8 (6)	4·5 (4)	5·0 (5)
		Monoclinic phase					Monoclinic phase			
Fit	R_B (%)	3·9	3·8	3·0	1·7	–	3·5	2·5	2·0	–
	% Monoclinic	61 (2)	60 (2)	53 (2)	47 (2)	–	70 (2)	52 (2)	44 (2)	–
	a (Å)	10·3022 (4)	10·2978 (4)	10·2610 (4)	10·1998 (3)	–	10·3191 (3)	10·2576	10·2210 (3)	–
	b (Å)	2·9567 (1)	2·9574 (1)	2·9603 (2)	2·9643 (2)	–	2·9600 (1)	2·9658 (1)	2·9710 (2)	–
	c (Å)	9·9295 (4)	9·9409 (4)	9·9880 (4)	10·0707 (3)	–	9·9146 (3)	9·9992 (4)	10·0639 (4)	–
	β (Å)	91·221 (3)	91·168 (3)	90·879 (3)	90·400 (2)	–	91·339 (2)	90·844 (3)	90·499 (3)	–
Ti1	x	0·3379 (8)	0·3375 (9)	0·3345 (8)	0·3335 (8)	–	0·3282 (6)	0·3343 (8)	0·3321 (10)	–
	z	0·1588 (9)	0·1576 (9)	0·1528 (10)	0·1490 (6)	–	0·1556 (8)	0·1529 (7)	0·1514 (8)	–
	B (Å^2)	1·4 (2)	0·2 (8)	1·7 (3)	1·1 (2)	–	0·4 (1)	0·45 (15)	0·7 (2)	–
Ti2	x	0·8567 (6)	0·8567 (6)	0·8540 (7)	0·8518 (5)	–	0·8466 (6)	0·8511 (7)	0·8546 (7)	–
	z	0·3349 (6)	0·3338 (6)	0·3316 (6)	0·3342 (4)	–	0·3323 (9)	0·3301 (8)	0·3291 (8)	–
	B (Å^2)	0·07 (14)	0·15 (15)	0·36 (15)	1·4 (2)	–	1·10 (15)	1·2 (2)	0·6 (2)	–
O1	x	0·2919 (4)	0·2916 (4)	0·2931 (5)	0·2968 (4)	–	0·2938 (5)	0·2956 (4)	0·2960 (4)	–
	z	0·3506 (4)	0·3499 (4)	0·3439 (4)	0·3446 (4)	–	0·3537 (5)	0·3464 (4)	0·3454 (5)	–
	B (Å^2)	0·16 (9)	0·20 (10)	1·00 (15)	0·9 (1)	–	1·25 (10)	0·75 (10)	−0·1 (1)	–
O2	x	0·0363 (3)	0·0370 (4)	0·0389 (4)	0·0404 (4)	–	0·0375 (3)	0·0396 (4)	0·0403 (4)	–
	z	0·3215 (4)	0·3224 (4)	0·3234 (5)	0·3286 (4)	–	0·3171 (4)	0·3244 (5)	0·3278 (5)	–
	B (Å^2)	−0·04 (8)	−0·05 (8)	0·8 (1)	1·05 (15)	–	−0·07 (10)	0·75 (11)	0·04 (15)	–
O3	x	0·6578 (3)	0·6579 (3)	0·6587 (4)	0·6611 (4)	–	0·6591 (4)	0·6555 (4)	0·6596 (6)	–
	z	0·0397 (4)	0·0391 (4)	0·0362 (3)	0·0395 (4)	–	0·0377 (4)	0·0385 (4)	0·0407 (5)	–
	B (Å^2)	−0·14 (8)	−0·15 (10)	−0·2 (1)	1·2 (1)	–	−0·15 (8)	0·25 (10)	−0·05 (15)	–
O4	x	0·6618 (3)	0·6616 (3)	0·6603 (4)	0·6584 (4)	–	0·6627 (4)	0·6587 (4)	0·6566 (5)	–
	z	0·3064 (4)	0·3060 (4)	0·3024 (3)	0·3011 (4)	–	0·3032 (4)	0·3030 (4)	0·3016 (4)	–
	B (Å^2)	0·0 (1)	−0·24 (10)	−0·20 (10)	0·7 (1)	–	0·43 (8)	0·44 (10)	−0·20 (15)	–
		Tetragonal phase					Tetragonal phase			
Fit	R_B (%)	3·0	3·2	2·8	1·9	1·7	2·6	2·3	2·1	2·1
	a (Å)	10·1205 (4)	10·1232 (3)	10·1307 (3)	10·1361 (1)	10·1434 (2)	10·1299 (4)	10·1353 (2)	10·1434 (2)	10·1479 (3)
	b (Å)	2·9561 (2)	2·9571 (2)	2·9598 (1)	2·96390 (5)	2·96795 (8)	2·9587 (1)	2·9636 (1)	2·9692 (1)	2·9730 (1)
Ti1	x	0·3333 (13)	0·3341 (11)	0·3314 (7)	0·3322 (4)	0·3331 (3)	0·3247 (19)	0·3318 (7)	0·3332 (6)	0·3329 (3)
	z	0·1539 (12)	0·1538 (10)	0·1492 (7)	0·1498 (4)	0·1495 (2)	0·1500 (14)	0·1506 (6)	0·1511 (6)	0·1492 (3)
	B (Å^2)	1·2 (3)	1·2 (2)	0·7 (1)	0·75 (10)	0·77 (4)	0·95 (15)	0·85 (10)	0·90 (10)	0·95 (5)
O1	x	0·3012 (6)	0·3012 (6)	0·3016 (4)	0·3005 (2)	0·2997 (1)	0·3058 (8)	0·3037 (4)	0·3022 (3)	0·3000 (2)
	z	0·3451 (9)	0·3460 (8)	0·3483 (4)	0·3473 (3)	0·3455 (2)	0·3476 (13)	0·3497 (4)	0·3488 (3)	0·3470 (2)
	B (Å^2)	2·6 (3)	2·8 (3)	1·1 (1)	0·8 (1)	0·70 (5)	1·05 (30)	1·15 (10)	0·9 (1)	0·65 (4)
O2	x	0·0303 (8)	0·0300 (7)	0·0388 (2)	0·0388 (2)	0·0385 (1)	0·0378 (9)	0·0398 (4)	0·0391 (3)	0·0387 (2)
	z	0·3354 (12)	0·3365 (10)	0·3317 (5)	0·3332 (3)	0·3326 (2)	0·3367 (13)	0·3341 (6)	0·3341 (5)	0·3324 (2)
	B (Å^2)	2·2 (5)	2·8 (3)	0·9 (1)	0·55 (10)	0·70 (5)	1·75 (35)	1·45 (10)	1·1 (3)	0·95 (5)

powder for instance, the goodness of fit $(R_{wp}/R_{wp}^E)^2$ is still greater than 2 when refined under the same conditions as the hollandites. It should be pointed out that no significant improvement in either R_B or R_{wp} for the hollandites was obtained by adopting $I2$ as the monoclinic space group rather than $I2/m$. Unlike Schmactel & Muller-Buschbaum (1980) the use of lower-symmetry space group was not considered to be justified. The structural coordinates given by refinement are presented in Table 1 according to the scheme,

Ba: 0 y 0 Ti and O: x 0 z.

In the tetragonal phases the coordinates for Ti2, O3 and O4 are omitted as these can be derived by symmetry from the coordinates for Ti, O2 and O1, respectively. The B parameters quoted for Ti and O should not be considered as accurate. In the first place no correction has been made for absorption. Also, some of the B values in the monoclinic phases are negative but these are highly correlated with the corresponding values in the tetragonal phases which are larger than expected. Furthermore, when a full Voigt function is fitted, rather than a pseudo-Voigt, some of the B values change quite significantly. Fortunately, the atomic coordinates of Ti and O are not strongly correlated with other parameters and are relatively insensitive to profile shape. The bulk of the discussion in this work is therefore based on parameters with uncorrelated errors namely the atomic coordinates of the Ti and O, and the lattice parameters.

Discussion of results

The compositions of the two specimens given by Rietveld refinement, 1·07 (3) and 1·31 (3) Ba per cell, are close to the values expected from the relative amounts of starting materials. These compositions are also consistent with the superlattice multiplicities

obtained from the 2θ positions of the $0k1/1k0$ X-ray superlattice line. In Ba(1·07) hollandite, this peak is at $2\theta = 17{\cdot}50°$ for Cu $K\beta$ radiation ($\lambda = 1{\cdot}3922$ Å) giving a multiplicity $m = 4{\cdot}70$; the value obtained by Kesson & White (1986) for concentrations between 1·08 and 1·14 Ba atoms per cell. In Ba(1·31) the same peak is at $2\theta = 18{\cdot}50°$ and $m = 5{\cdot}30$ which would suggest a concentration > 1·25 Ba atoms per cell on the assumption that m is normally in the range 5·7 to 5·8 at 1·33 Ba atoms per cell. The monoclinic lattice parameters for Ba(1·07) at 300 K are similar to those obtained by Kesson & White (1986) for $Ba_{1\cdot14}Ti_8O_{16}$ at room temperature. Conversely, the lattice parameters quoted by Schmactel & Muller-Buschbaum (1980) for '$BaTi_8O_{16}$' are comparable to the present results for the Ba(1·31) hollandite at 298 K. Their specimen probably corresponds to an actual composition close to 1·33 Ba atoms per cell.

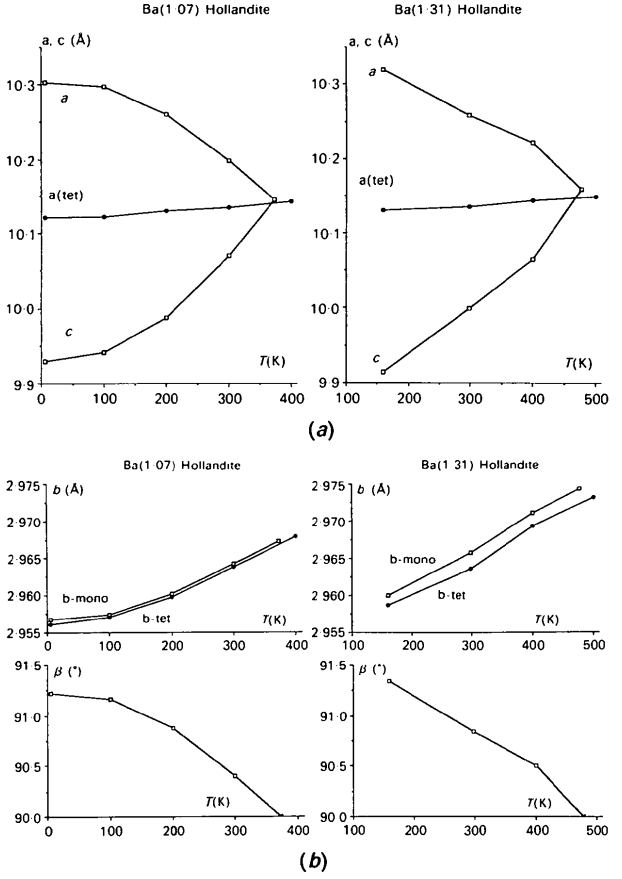

Fig. 3. Lattice parameters for $Ba_xTi_8O_{16}$ at $x = 1{\cdot}07$ and 1·31 plotted as a function of temperature. The abbreviations 'mono' and 'tet' refer to monoclinic and tetragonal. No error bars are included as these are covered by the plotted symbols. (*a*) Monoclinic parameters *a* and *c* and tetragonal parameter *a*. In both lattices the *b* axis is taken as the unique axis. (*b*) Monoclinic parameters *b* and β and tetragonal parameter *b* (unique axis).

The lattice parameters *a*, *b*, *c* and β for the monoclinic and tetragonal phases in the present specimens are plotted as a function of temperature in Figs. 3(*a*) and 3(*b*). Error bars are not plotted on these graphs as all the e.s.d.'s are within the limits $\sigma(a)$ and $\sigma(c) \leq 0{\cdot}0004$ Å and $\sigma(b) \simeq 0{\cdot}0001$ Å, and are encompassed by the plotting symbols. In both tetragonal phases the lattice parameters vary smoothly and monotonically over the complete temperature range. Both sets of monoclinic **a** and **c** parameters converge uniformly to the condition $a = c$ at $\beta = 90°$ at their respective transition temperatures T_c. Up to each transition temperature the monoclinic *b* parameter is larger than the corresponding tetragonal *b* parameter by a constant amount. Δb is approximately 0·0005 Å for Ba(1·07) and 0·0020 Å for Ba(1·31). When the monoclinic parameters *a* and *c* are plotted against the monoclinic angle β the plots are distinctly linear and both *a* and *c* converge to the same value at $\beta = 90°$. This intercept value is used in Fig. 3(*a*) to identify the *a* and *c* value of each monoclinic phase at $T = T_c$. At T_c the estimated *a* ($= c$) value is larger than the corresponding tetragonal value of *a* at T_c by 0·0043 Å for Ba(1·07) and 0·0115 Å for Ba(1·31). With the exception of β, the monoclinic lattice parameters *a*, *b* and *c* all undergo a discontinuous change at T_c. This change represents discontinuous contractions in the (010) plane and along the [010] tunnel direction giving an overall volume contraction. The cell volume V_c is plotted as a function of temperature in Fig. 4 along with the linear coefficient of expansion along the tunnel direction $\alpha_b = (1/b)(db/dT)$ and the volume coefficient of expansion $\gamma_v = (1/V_c)(dV_c/dT)$. The continuous curves for V_c, α_b and γ_v plotted in Fig. 4 were obtained by fitting cubic polynominals to the data

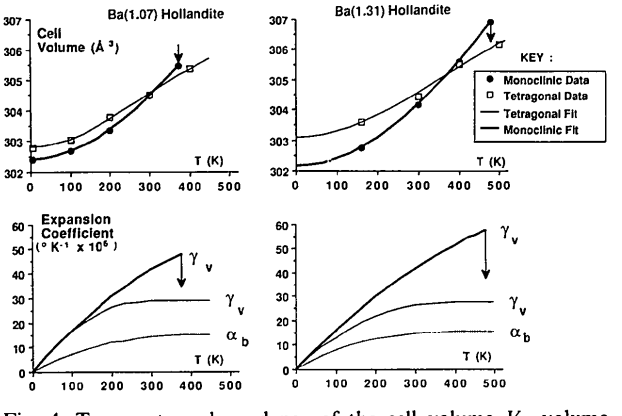

Fig. 4. Temperature dependence of the cell volume V_c, volume expansion coefficient γ_v and the linear coefficient of expansion along the tunnel α_b for the monoclinic and tetragonal phases in $Ba_{1\cdot07}Ti_8O_{16}$ and $Ba_{1\cdot31}Ti_8O_{16}$. The plots for γ_v and α_b were calculated from lines fitted to V_c and *b*. The coefficient α_b is the same for the monoclinic and tetragonal phases.

Table 2. *Transformation characteristics of the* Ba(1·07) *and* Ba(1·31) *hollandites at the transition temperatures* T_c

The symbols used in this table are the cell volume V_c, the lattice parameter b, the volume coefficient of expansion $\gamma_v = (1/V_c)(dV_c/dT)$, and (M) and (T), which refer to the monoclinic and tetragonal phases, respectively. All the changes, ΔV_c, Δb and $\Delta\gamma_v$, assume the temperature is increasing.

	T_c (K)	V_c(M) (Å^3) V_c(T) (Å^3)	ΔV_c (%)	b(M) (Å) b(T) (Å)	Δb (%)	γ_v(M) (K^{-1}) γ_v(T) (K^{-1})	$\Delta\gamma_v$ (%)
$Ba_{1\cdot07}Ti_8O_{16}$	375	305·46 305·15	−0·10	2·9673 2·9668	−0·017	48×10^{-6} 26×10^{-6}	−46
$Ba_{1\cdot31}Ti_8O_{16}$	475	306·92 306·02	−0·29	2·9742 2·9722	−0·067	58×10^{-6} 25×10^{-6}	−57

for the cell volume and b, with the thermodynamic constraints, $dV_c/dT = 0$ and $db/dT = 0$ at $T = 0$ K, imposed on the fitting procedure [*i.e.* V_c (or b) $= a_0 + a_1T^2 + a_2T^3$]. Values for V_c and b obtained by extrapolating the monoclinic parameters to $\beta = 90°$ were included as data points at $T = T_c$. A summary of the discontinuous changes in the various lattice parameters and expansion coefficients at the transition temperatures is presented in Table 2.

The biggest contribution to the change in cell volume ΔV_c on transition arises from changes within the (010) plane. This is expected as the monoclinic distortion occurs in this plane. The small change in the tunnel-lattice parameter b is probably a second-order effect of the change in distortion. Although the degree of distortion is significantly different, the actual difference in cell volumes between the monoclinic phases in Ba(1·07) and Ba(1·31) is small. The monoclinic b parameters as well as the monoclinic cell volumes extrapolate back to approximately the same values at 0 K [*i.e.* $b = 2{\cdot}9565\,(1)$ and 2·9568 (3) Å, $V_c = 302{\cdot}40\,(2)$ and 302·15 Å^3 for Ba(1·07) and Ba(1·31) respectively]. This similarity suggests that at 0 K V_c and b are largely independent of the cation content of the structure and dependent primarily on the packing of the O atoms. A possible explanation is that the Ba and Ti ions are smaller than the spaces they occupy in the oxygen polyhedra and at 0 K the cell dimensions are limited by O—O contact rather than Ba—O or Ti—O contact.

A number of features of the expansion should be highlighted. Only the monoclinic phases display any significant increase in γ_v with temperature and in both cases γ_v drops by approximately 50% on transformation. Also, the volume expansion of each monoclinic phase is independent of Ba concentration over the common temperature range [*i.e.* $\gamma_v(1{\cdot}07,\mathrm{M}) \simeq \gamma_v(1{\cdot}31,\mathrm{M})$ where M = monoclinic]. The same is true of the volume expansion of the tetragonal phases [*i.e.* $\gamma_v(1{\cdot}07,\mathrm{T}) \simeq \gamma_v(1{\cdot}31,\mathrm{T})$ where T = tetragonal]. Along the tunnel direction the linear expansion is not only independent of the Ba concentration it is also independent of the symmetry [*i.e.* $\alpha_b(\mathrm{M}) \simeq \alpha_b(\mathrm{T})$]. Both monoclinic phases expand more or less isotropically in that the volume expansion $\gamma_v \simeq 3\alpha_b$ where α_b is the linear-expansion coefficient along the tunnel axis. Above each T_c however, the expansion is anisotropic and over 50% of the volume expansion arises from linear expansion along the tunnel axis. Above 250 K the linear expansion α_b of all the phases is similar and constant at $\alpha_b = 15\,(2) \times 10^{-6}$ K^{-1}. This is similar to the tetragonal hollandite $Ba_{1\cdot14}(Al_{2\cdot28}Ti_{5\cdot72})O_{16}$ which expands isotropically with a linear-expansion coefficient of $11\,(1) \times 10^{-6}$ K^{-1} up to 1200 K (Sabine & Hewat, 1982).

Both hollandites display first-order transition characteristics; the cell volume is discontinuous on transition and both phases coexist below the transition temperature. This type of transition is often associated with some form of diffusion activity involving interchange of atoms or changes where the first coordination bonds are broken and reformed. As structural parameters are available for both the equilibrium monoclinic phases and the metastable tetragonal phases, it is possible to examine how specific parts of the hollandite structure change with increasing temperature and on transformation. Basically each hollandite unit cell consists of two sets of oxygen polyhedra; eight oxygen octahedra enclosing Ti ions and two box-shaped cavities of O atoms surrounding A sites containing either Ba ions or vacancies. The manner in which the volumes of these oxygen polyhedra vary with temperature is shown in Fig. 5 for both phases. There are a number of notable features in these graphs:

(i) In both monoclinic phases the volume of the oxygen octahedra is almost independent of temperature. The same octahedra in the tetragonal phases contract with temperature above 200 K. The tunnel cavities in all phases on the other hand display a normal expansion behaviour above 200 K.

(ii) In Ba(1·31) hollandite the oxygen octahedra are larger than the corresponding Ba(1·07) octahedra. This is expected because of the larger proportion of Ti^{3+} in the Ba(1·31) hollandite. According to Shannon (1976) the Ti^{4+}—O bond $\simeq$ 1·98 and Ti^{3+}—O $\simeq$ 2·05 Å. Despite the larger Ba occupancy and associated Ti^{3+} content, the tunnel cavities in the Ba(1·31) hollandite are smaller than those in Ba(1·07). Normally, the cavity volume increases in

unison with the octahedral volume (Cheary, 1986). In this instance the higher linear charge density of Ba^{2+} ions in the tunnels of Ba(1·31) must be exerting an electrostatic pull on the O4 and O1 atoms strong enough to counteract the expansion caused by the wall enlargement.

(iii) On transformation from monoclinic to tetragonal there is a discontinuous increase in the octahedral volume [*i.e.* $\Delta V_{oct}/V_{oct} \simeq +1{\cdot}5\%$ for Ba(1·07) and +2% for Ba(1·31)]. The observed decrease in cell volume on transformation arises from a large decrease in the volume of the tunnel cavities [*i.e.* $\Delta V_{cav}/V_{cav} \simeq -2\%$ for Ba(1·07) and −3% for Ba(1·31)].

In general terms it would appear that the conversion from monoclinic to tetragonal is a relaxation of a shear strain on the tunnel walls. In this process the oxygen octahedra expand and the thickness of each tunnel wall, represented by the separations $O1_1$—$O1_4$ and $O4_4$—$O4_1$, increases by ~0·04 Å thereby causing the tunnel cross-section to contract. The capacity of the oxygen octahedra to be compressed comes about because the enclosed volume is not completely filled by the Ti ions which in all cases are off-centre by amounts ranging from 0·07 to 0·16 Å. An illustration of the wall-relaxation process is provided in Fig. 6 which shows the oxygen frameworks around each tunnel in the monoclinic and tetragonal phases of Ba(1·07) at 5 K. Both walls undergo a shear strain in the tetragonal to monoclinic conversion as if acted on by an equal and opposite force in the [101] and [10$\bar{1}$] direction as shown. This type of strain is limited by O—O contact between atoms on the opposite faces of the wall. In the S walls of the monoclinic phases the pairs $O1_4$—$O2_4$ and $O1_1$—$O2_1$ are in relatively close contact at between 2·60 and 2·63 Å. The same is true of the corresponding O atoms in the T walls. In the tetragonal state the separation of these O pairs is larger by up to 0·12 Å as the shear strain is removed.

It is evident that the monoclinic distortion is more complex than the simple process of the corner O atoms O2 and O3 acting as hinges and producing equal and opposite changes in φ and ψ relative to the tetragonal state ($\varphi = \psi$). The hinge angles φ and ψ behave quite differently, as shown in Fig. 7. On transformation to tetragonal φ undergoes a very sharp decrease by up to 4° whereas ψ is continuous. A puzzling and possibly related phenomenon is the temperature dependence of the mean Ti—O bond length ⟨Ti—O⟩ in the S and T octahedra. This is shown in Fig. 8 along with ⟨Ti—O⟩ bond lengths in the tetragonal phases. Unlike $Ba_x(Mg_xTi_{8-x})O_{16}$

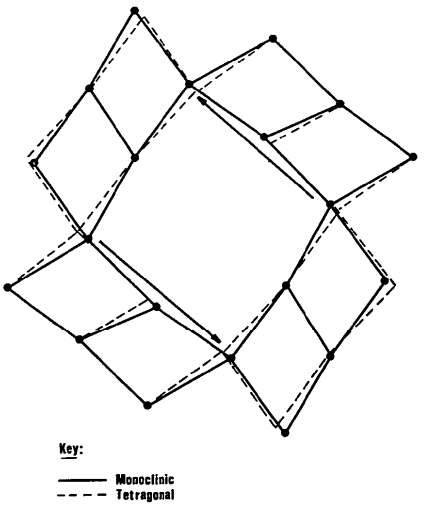

Fig. 6. A comparison of the oxygen framework in the tetragonal and monoclinic phases of $Ba_{1\cdot07}Ti_8O_{16}$ at 5 K. The transformation, tetragonal to monoclinic, corresponds to a shearing strain as if acted on by forces in the direction shown.

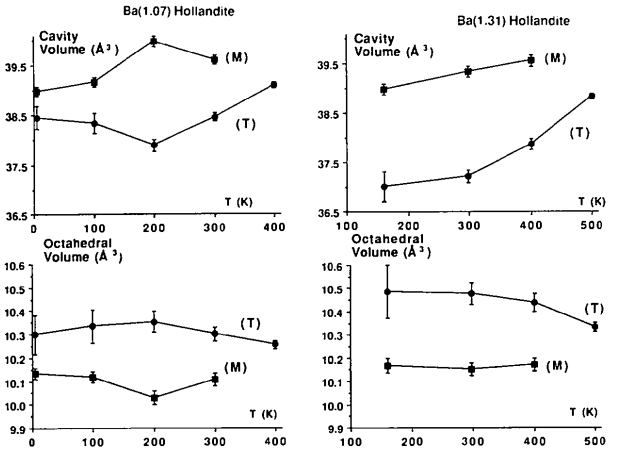

Fig. 5. Temperature dependence of the average volume per oxygen octahedron and the *A*-site cavity volume for the monoclinic and tetragonal phases of $Ba_{1\cdot07}Ti_8O_{16}$ and $Ba_{1\cdot31}Ti_8O_{16}$. In the diagram M = monoclinic and T = tetragonal.

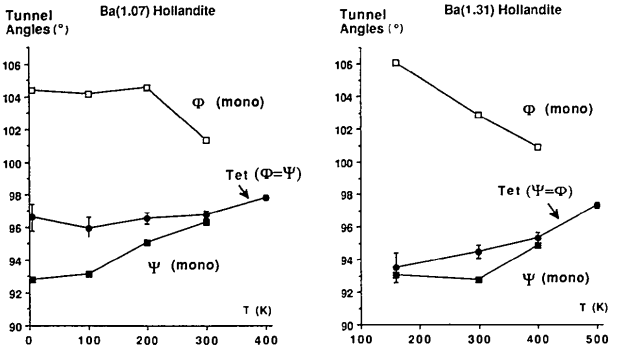

Fig. 7. The hinge angles φ and ψ (see Fig. 1) plotted as a function of temperature for the tetragonal and monoclinic phases of $Ba_{1\cdot07}Ti_8O_{16}$ and $Ba_{1\cdot31}Ti_8O_{16}$. In the tetragonal phase $\varphi = \psi$.

hollandites, the ⟨Ti—O⟩ bond length in the T octahedra is longer than in the S octahedra at room temperature. At 0 K the situation is reversed and the ⟨Ti—O⟩ bond length is longer in S octahedra. In the vicinity of $T \simeq 0{\cdot}5$–$0{\cdot}6T_c$ the ⟨Ti—O⟩ bond length in the S octahedra of both hollandites passes through a minimum. A possible explanation of this behaviour is a temperature-dependent and different $\langle Ti^{3+}/Ti^{4+}\rangle$ ratio on the S and T sites. These compounds are semiconducting with an energy gap of approximately 0·1 eV and changes in the $\langle Ti^{3+}/Ti^{4+}\rangle$ ratio in a particular tunnel wall could occur by electron transfer between walls. To maintain charge balance a transfer mechanism such as this would be manifested by equal and opposite changes in the ⟨Ti—O⟩ bond lengths of the S and T octahedra. Although the results for Ba(1·31) display some degree of mirror symmetry in the S and T bond lengths, the results for Ba(1·07) do not, as the decrease in the S bond length is approximately four times the increase in the T bond length over the range 0–200 K. It would be incorrect therefore, to assume that the ⟨Ti—O⟩ bond length in the present hollandites is controlled solely by the $\langle Ti^{3+}/Ti^{4+}\rangle$ ratio in the octahedra. In both hollandites the ⟨Ti—O⟩ bond length in the tetragonal phase is bigger than the bond lengths in the S and T octahedra of the monoclinic phase even though the composition is the same. As indicated earlier, the oxygen octahedra are under compression in the monoclinic state owing to closer contact of the O1 and O4 atoms with the Ba ions in the tunnels. In the monoclinic state the difference in the ⟨Ti—O⟩ bond lengths of the S and T octahedra and, possibly the behaviour of the hinge angles φ and ψ, is the result of different stresses on each of the octahedral walls. The temperature dependence of the ⟨Ti—O⟩ bond lengths in this case will be dominated by the vibration of the Ti and O atoms only at high temperatures. At low temperatures the contraction of the ⟨Ti—O⟩ bond in the S octahedra is linked to the expansion of the tunnel cavities and is manifested as a reduction of the Ti—O1$_4$ bond.

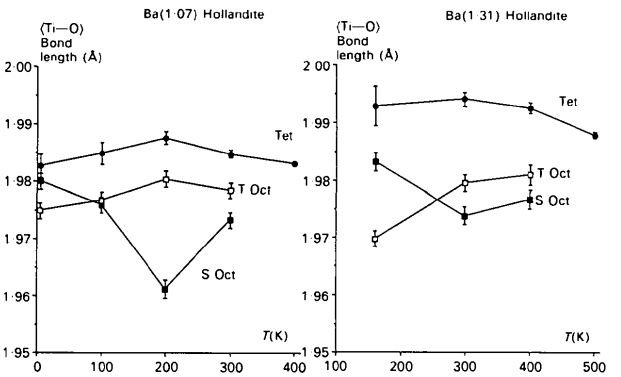

Fig. 8. The mean Ti—O bond lengths per oxygen octahedra plotted as function of temperature for $Ba_{1\cdot07}Ti_8O_{16}$ and $Ba_{1\cdot31}Ti_8O_{16}$. In the plots, 'tet' refers to the tetragonal phase, 'S Oct' refers to the S octahedra and 'T Oct' refers to the T octahedra in the monoclinic phases.

$Ba_xTi_8O_{16}$ hollandites are unusual in that they are the only ones amongst the nominally monoclinic hollandites [*e.g.* Ba_x(Fe/Ti), Ba_x(Ni/Ti) and Ba_x(Mg/Ti) hollandites] in which the high-temperature tetragonal phase coexists along with the monoclinic phase. All of the examples quoted have transitions in the same temperature domain as the Ti^{3+} based hollandites (*i.e.* $T_c = 350$–650 K) and presumably the same transformation mechanism operates. As the transformation involves a shear strain, probably without cation migration, the presence of a two-phase mixture can be interpreted as some crystallites being unable to transform to monoclinic on cooling. Barriers to propagation of the strain throughout the crystallites could possibly arise from defects or impurities induced by interstitial hydrogen diffused in during preparation. This would account qualitatively at least for the weight fractions of monoclinic phase being temperature dependent only and reasonably reproducible on cycling the temperature between room temperature and 5 K. The martensitic transformation in ZrO_2 at 1445 K displays a number of similar characteristics to the present materials. Firstly, the transformation, going from high temperature to low temperature, is from tetragonal to monoclinic and there is a volume increase in this direction. The transformation is athermal. This means that the transformation occurs over a range of temperatures and the amount of transformed phase depends on the temperature alone and does not change with time (Subbarao, 1981). One explanation of this is that small crystallites ($\simeq$2000 Å) transform at a lower temperature because the surface energy holds back the deformation and expansion associated with the transformation. Lack of defects in ZrO_2, particularly dislocation clusters, can also suppress nucleation of the monoclinic phase and tetragonal ZrO_2 particles can exist down to 4·2 K (Chen & Chiao, 1984). With impurities such as Y, Ca and Mg in ZrO_2, the tetragonal phase is retained at room temperature and transformation to monoclinic is induced by mechanical rather than thermal stress. In view of the similarities between the transition in ZrO_2 and that in the present samples, electron-microscopy studies are being undertaken to establish whether or not the hollandite transformation is martensitic. In addition, high-temperature X-ray studies are being carried out to determine the transformation characteristics of a broad range of barium hollandites.

In the context of nuclear-waste disposal, $Ba_xTi_8O_{16}$ is used because it can accommodate a high concentration of Cs and retain it at temperatures up

Table 3. *Tunnel-cavity dimensions at room temperature in* $Ba_xTi_8O_{16}$ ($x = 1{\cdot}07$ *and* $1{\cdot}31$) *and* $Ba_x(Ti/M)_8O_{16}$ *hollandites with* M = Al, Ga, Fe *and* Mg *[from Cheary* (1986) *and Cheary & Squadrito* (1989)]

In the table $\langle A—O\rangle$ refers to the mean distance between the centre of the tunnel cavity and the eight surrounding O atoms and $\langle O—O\rangle$ refers to the mean separation across the diagonal of the planar array of O atoms at the top and bottom of the cavity (*i.e.* $O1_4—O1_3$ and $O4_3—O4_4$ distances).

Hollandite	$\langle A—O\rangle$ (Å)	Cavity volume (Å^3)	$\langle O—O\rangle$ (Å)	Room temp. symmetry
$Ba_{1{\cdot}07}Ti_8O_{16}$	2·98	39·6	5·17	Monoclinic
$Ba_{1{\cdot}31}Ti_8O_{16}$	2·98	39·35	5·16	Monoclinic
$Ba_{1{\cdot}14}(Mg/Ti)_8O_{16}$	2·96	39·0	5·12	Monoclinic
$Ba_{1{\cdot}28}(Fe/Ti)_8O_{16}$	2·96	38·95	5·12	Monoclinic
$Ba_{1{\cdot}26}(Ga/Ti)_8O_{16}$	2·94	38·25	5·08	Tetragonal
$Ba_{1{\cdot}14}(Al/Ti)_8O_{16}$	2·93	37·6	5·07	Tetragonal
$Ba_{1{\cdot}23}(Al/Ti)_8O_{16}$	2·92	37·25	5·05	Tetragonal

to 600 K. To do this the tunnel cavity must be large enough to accept a Cs—O bond length typically 3·0–3·2 Å in eightfold coordination. At room temperature the tunnel-cavity volume and mean distance from the centre of the cavity to neighbouring O atoms in $Ba_{1{\cdot}07}Ti_8O_{16}$ are 39·6 and 2·98 Å. These values indicate that Cs is accommodated without considerable deformation being developed around the tunnels. The size of the A-site cavity in the present hollandites is larger than any other Ba(M/Ti) hollandites for which structural data is available (see Table 3). In $Ba_{1{\cdot}14}(Al^{3+}/Ti^{4+})O_{16}$, only 0·25 Cs atoms per cell can be substituted for Ba under normal atmospheric pressure conditions but in $Ba_{1{\cdot}07}(Ti^{3+}/Ti^{4+})_8O_{16}$ up to 1·32 Cs can be substituted even though the cavity volume is only 5% larger. Besides being able to accommodate large ions in the tunnels it is equally important to retain them at high temperatures. This will be determined by how easily they can jump out of their sites and become mobile along the tunnels. To inhibit migration the size of the hole in the square-planar array of oxygens $O1_4—O4_4—O1_3—O4_3$ forming the top and bottom of each tunnel cavity should be smaller than the diameter of the Ba cation. Alternatively, the mean diagonal O—O distance across the planar group (*i.e.* the mean of $O1_4—O1_3$ and $O4_3—O4_4$) needs to be smaller than 2 × (Ba—O) bond length. In tetragonal $Ba_{1{\cdot}07}Ti_8O_{16}$ the $\langle O—O\rangle$ diagonal distance varies linearly with temperature above 200 K and extrapolates to 5·6 Å [*i.e.* 2 × (Ba—O) bond length] between 1100 and 1300 K. In this temperature range the activation energy of the Ba ion will be small and the ion should be quite mobile and no longer ordered on the A sites. The $\langle O—O\rangle$ diagonal distances of a range of $Ba_x(M/Ti)_8O_{16}$ hollandites at room temperature are compared with the $Ba_xTi_8O_{16}$ hollandites in Table 3. The effect of temperature on the ordering of Ba and Cs in various hollandites is currently being investigated, through an analysis of the X-ray superlattice line intensities, to identify and characterize the order–disorder transition.

I wish to acknowledge the financial support provided for this work by the Australian Nuclear Science and Technology Organization under research contract No. 82/X/1. I am also indebted to the Institut Laue–Langevin and in particular Dr Alan Hewat for providing access to the excellent facilities at this laboratory. Many thanks are also extended to the Powder Diffraction Group at the SERC Synchrotron Laboratory, Daresbury, England.

References

BURSILL, L. A. & GRZINIC, G. (1980). *Acta Cryst.* **B36**, 2902–2913.

CADEE, M. C. & VERSCHOOR, G. C. (1978). *Acta Cryst.* **B34**, 3554–3558.

CHEARY, R. W. (1986). *Acta Cryst.* **B42**, 229–236.

CHEARY, R. W. (1987). *Acta Cryst.* **B43**, 28–34.

CHEARY, R. W. & SQUADRITO, R. (1989). *Acta Cryst.* **B45**, 205–212.

CHEN, I. W. & CHIAO, Y. H. (1984). *Adv. Ceram.* **12**, 33–45.

CLARK, S. M. (1989). *Nucl. Instrum. Methods Phys. Res. A*, **276**, 381–387.

FANCHON, E., VICAT, J., HODEAU, J. L., WOLFERS, P., TRAN QUI, D. & STROBEL, P. (1987). *Acta Cryst.* **B43**, 440–448.

FIELDING, P. E. & WHITE, T. J. (1987). *J. Mater. Res.* **2**, 387–414.

HEWAT, A. (1986). *Mater. Sci. Forum*, **9**, 69–80.

HOWARD, C. J. (1982). *J. Appl. Cryst.* **15**, 615–620.

HOWARD, C. J. & HILL, R. J. (1986). Report AAEC/M112. Australian Atomic Energy Commission, Lucas Heights Research Laboratories, Australia.

KESSON, S. E. (1983). *Radioact. Waste Manage.* **4**, 53–72.

KESSON, S. E. & WHITE, T. J. (1986). *Proc. R. Soc. London Ser. A*, **405**, 73–101.

MIJLHOFF, F. C., IJDO, D. J. W. & ZANDERBERGEN, H. W. (1985). *Acta Cryst.* **B41**, 98–101.

ROTH, R. (1981). Annual Report NBSIR81-2241. National Measurements Laboratory, Office of Nuclear Technology, Australia.

SABINE, T. M. & HEWAT, A. (1982). *J. Nucl. Mater.* **110**, 173–177.

SCHMACTEL, J. & MULLER-BUSCHBAUM, H. K. (1980). *Z. Naturforsch. Teil B*, **35**, 332–334.

SHANNON, R. D. (1976). *Acta Cryst.* **A32**, 751–767.

SUBBARAO, E. C. (1981). *Adv. Ceram.* **3**, 1–24.

WILES, D. B. & YOUNG, R. A. (1981). *J. Appl. Cryst.* **14**, 149–150.

WYCKOFF, R. W. G. (1963). *Crystal Structures*, Vol. I. New York: Wiley–Interscience.

ZANDERBERGEN, H. W., EVERSTIJN, P. L. A., MIJLHOFF, F. C., RENES, G. H. & IJDO, D. J. W. (1987). *Mater. Res. Bull.* **22**, 431–438.